Organic salts as super-high rate capability materials for lithium-ion batteries

Y. Y. Zhang, Y. Y. Sun, S. X. Du, H.-J. Gao, and S. B. Zhang

Related Articles

First-principles study of transition metal doped Li2S as cathode materials in lithium batteries
J. Renewable Sustainable Energy 4, 063128 (2012)

First-principles study of the oxygen adsorption and dissociation on graphene and nitrogen doped graphene for Li-air batteries
J. Appl. Phys. 112, 104316 (2012)

Diffusion-induced stresses of electrode nanomaterials in lithium-ion battery: The effects of surface stress
J. Appl. Phys. 112, 103507 (2012)

Delineating local electromigration for nanoscale probing of lithium ion intercalation and extraction by electrochemical strain microscopy
Appl. Phys. Lett. 101, 063901 (2012)

Impedance spectroscopy of the superprotonic conduction in LiH2PO4
Appl. Phys. Lett. 101, 012905 (2012)

Additional information on Appl. Phys. Lett.

Journal Homepage: http://apl.aip.org/

Journal Information: http://apl.aip.org/about/about_the_journal

Top downloads: http://apl.aip.org/features/most_downloaded

Information for Authors: http://apl.aip.org/authors

Organic salts as super-high rate capability materials for lithium-ion batteries

Y. Y. Zhang,[1,2] Y. Y. Sun,[2] S. X. Du,[1] H.-J. Gao,[1] and S. B. Zhang[2,a]
[1]Institute of Physics, Chinese Academy of Sciences, P.O. Box 603, Beijing 100190, China
[2]Department of Physics, Applied Physics and Astronomy, Rensselaer Polytechnic Institute, Troy, New York 12180, USA

First-principles calculation reveals that organic salts could be super-high rate capability electrode materials for Li-ion batteries. We show that di-lithium terephthalate, an anode material demonstrated recently by experiment, has low Li diffusion barrier (E_A). A resonant bonding model for the low E_A is developed, which leads to the prediction that di-potassium terephthalate (K_2TPA) has even lower E_A (150 meV), with diffusion rate orders of magnitude higher than that in Li-intercalated graphite. The calculated anode voltage (0.62 V), specific energy density (209 mA·h/g), and volume change upon lithiation (5%) make K_2TPA a promising anode material for power-intensive applications such as electric-vehicles. © 2012 American Institute of Physics. [http://dx.doi.org/10.1063/1.3689764]

Lithium-ion batteries (LIBs) hold great potential for powering electric vehicles (EVs) owing to their high energy density. Different from applications in portable electronic devices, power-intensive applications, such as in EVs, also require high charge/discharge rate in addition to high energy density. The charge/discharge rate is largely determined by the Li diffusion coefficients within the electrodes and electrolyte, which are in turn determined by the activation barrier E_A for Li diffusion. According to experiment and first-principles calculation,[1–3] E_A in typical anode (e.g., Li-intercalated graphite or LiC_6) and cathode (e.g., $LiCoO_2$) materials is in the range of 300–400 meV. Enhancing the rate capability is usually achieved by nano engineering.[4–7] Recently, it has been proposed that a rational design of the crystal structure could also improve the rate capability of bulk electrode materials. High-rate cathode material, $Li(Ni_{0.5}Mn_{0.5})O_2$, has been reported based on such a design.[8] However, to date few anode material with rate capability higher than graphite has been reported.

Using first-principles calculations, we show that di-lithium terephthalate ($Li_2C_8H_4O_4$ or Li_2TPA) is a high rate capability material. Our study is motivated by a recent experimental report on Li_2TPA anode material, showing good performance on thermal stability, voltage profile, cyclability, capacity, and eco-efficiency.[9] The storage of Li in the organic salts is different from traditional battery materials by utilizing multiple valences of the organic groups. As illustrated in Fig. 1, the storage mechanism involves breaking aromatic π-bond in the benzenoid ring and regrouping the electrons into a set of new π-bonds. Noticeably, Li in this molecule is bistable and changes its registry in the presence of a Li vacancy. This is a property of the resonant bonding of COO ligand (see Fig. 1(a)), which not only merely lowers the energy at the transition state (i.e., the saddle point along the Li diffusion path) but also converts the saddle point to an energy minimum. In bulk Li_2TPA, E_A is only 210 meV, considerably lower than that of LiC_6 (calculated to be 390 meV), which is currently the dominant anode material. Using the

model, we predict that E_A in di-potassium terephthalate (K_2TPA) can be further lowered to only 150 meV. Compared with Li_2TPA, bulk K_2TPA has a more direct Li diffusion path and its transition state is unambiguously an energy minimum instead of a saddle point. Our results suggest that organic salts could be candidate materials in replacing Li-intercalated graphite as anode for high rate capability applications of LIBs.

Our calculations are based on the density functional theory (DFT) within the generalized gradient approximation (GGA), as implemented in the Vienna Ab-initio Simulation Package (VASP).[10–12] The exchange-correlation functional is that of Perdew and Wang (PW91).[13] We have tested the PW91 functional using Li-intercalated graphite and found that the anode voltage at full charge (i.e., LiC_6) is 0.10 V, which is in good agreement with experiment[14] and previous calculations.[2,15,16] The PW91 functional also performs the best among various pure GGAs in studying weak interacting systems.[17] We also performed DFT-D calculations,[18] which explicitly include the van der Waals (vdW) interaction by using a parameterized dispersion force field. Core electrons were represented by the projector augmented wave (PAW) potentials.[19] The 1s electrons of C and O and the 1s, 2s, and 2p electrons of K were treated as core electrons, while all electrons of Li are treated as valence electrons. The PAW cutoff radii are 0.582, 0.794, 0.804, 1.085, and 1.217 Å for H, C, O, Li, and K, respectively. Planewaves with cutoff energy at 520 eV were used as the basis set. Monkhorst-Pack[20] $2 \times 6 \times 2$ k-point grid was used to sample the
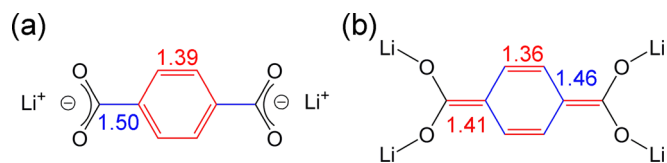
FIG. 1. (Color online) Li storage and diffusion mechanisms: (a) bonding before lithiation where the benzenoid ring is aromatic and each Li is shared by two O atoms, and (b) bonding after lithiation where the aromaticity of the benzenoid ring is removed. The calculated bond lengths for Li_2TPA shown in the figure (in Å) verify the C=C double bond assignments. Note that Li changes position before and after lithiation.

a)Author to whom correspondence should be addressed. Electronic mail: zhangs9@rpi.edu.
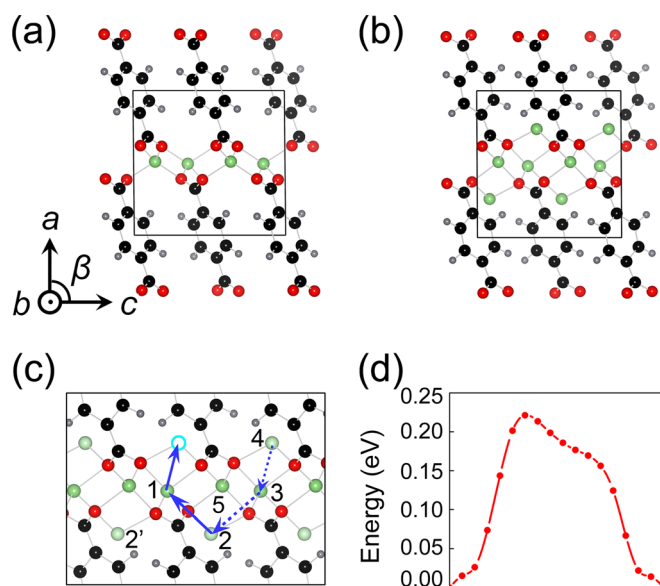
FIG. 2. (Color online) Crystal structure of Li$_2$TPA before (a) and after (b) lithiation. The Li, O, C, and H are denoted by green (light gray in black-and-white print version), red (gray), black, and small gray balls, respectively. Solid frames are the unit cells. Two types of Li present in this case, and they are given in slightly different colors. (c) Diffusion path of Li vacancy in Li$_2$TPA-Li$_2$. Open circle represents the initial Li vacancy. (d) Potential energy curve along the diffusion path calculated at 16 NEB images. Note that the curve is for a concerted motion where Li-1 moves to the vacancy while Li-2 simultaneously moves to the vacant Li-1 site.

Brillouin zone. Both the cell dimensions and atomic positions were optimized[21,22] until the forces are smaller than 0.01 eV/Å.

Li$_2$TPA crystallizes in monoclinic structure,[23] as shown in Fig. 2(a). To study the lithiation of Li$_2$TPA crystal, we selected ten possible initial structures with inserted Li. They were optimized by variable-cell relaxation, upon which the ten evolved into only two structures. The lower-energy one is shown in Fig. 2(b). To avoid the possibility that lower-energy structures are missed in the search using multiple starting configurations, we also carried out simulated annealing based on molecular dynamics calculations. The annealing starts with a configuration far from the stable one shown in Fig. 2(b), i.e., having all Li atoms sandwiched between the benzenoid rings. The system was then cooled down from 500 K to 0 K in 10 ps with 1 fs time steps. Our analysis indicates that the Li trajectories during the simulation have covered a sufficiently large phase space. Despite that, the final structure at 0 K was found to be the one shown in Fig. 2(b).

The lithiation of Li$_2$TPA takes place in the scheme shown in Fig. 1. As mentioned earlier, it involves the breaking of a π bond in the benzenoid ring (in the Kekule picture) and subsequent reshuffling of the remaining π bonds. The flexibility in breaking and reshuffling the π-bonds reflects the resonant nature of the bonds and multiple valences of the TPA molecule in forming the bonds with Li. This proposed lithiation process can be clearly verified by comparing the bond lengths before and after the lithiation, as shown in Fig. 1. For the sake of clarity, only the TPA molecule and the attached Li atoms are shown in Fig. 1. The bond lengths are, however, extracted from the calculations on the actual materials, instead of isolated molecules. It can be seen that the length of the C=C double bonds is in the range from

1.36 to 1.41 Å, while those of the C−C single bonds are significantly longer in the range from 1.46 to 1.50 Å.

Using the climbing-image nudged elastic band (NEB) method,[24,25] we studied Li diffusion. Li$_2$TPA can be viewed as a layered solid, in which Li diffusion primarily takes place in the *b-c* plane. A $1 \times 2 \times 2$ supercell with a $2 \times 2 \times 1$ *k*-point grid and a 400 eV cutoff for the plane-wave basis set were used in the NEB calculations. Here, we consider the diffusion as a diffusion of Li vacancy[26] in fully lithiated Li$_2$TPA (or Li$_2$TPA-Li$_2$), which is a valid approach for the initial stage of discharge. Usually, E_A decreases when more Li are delithiated.[26] There are two inequivalent Li sites in Li$_2$TPA-Li$_2$ and, correspondingly, two different Li vacancy sites. These two types of Li sites are marked by even and odd numbers, respectively, in Fig. 2(c). Our calculation shows that the vacancy at an odd-numbered site is not stable because the Li atom at a neighboring even-numbered site will fill the vacancy without any barrier, which results in a vacancy at the even-numbered site. We have considered the diffusion of each neighboring Li atom into the even-numbered vacant site. Figure 2(c) shows the minimum barrier path. In step I, Li-1 hops to fill the vacancy. In step II, either Li-2 or Li-2′ can hop to fill the vacancy left by Li-1 with equal probability. Here, we assume that it is Li-2. In step III, Li-3 hops to fill the vacancy left by Li-2, as a mirror process to step I. In step IV, we can bring the vacancy, as a mirror process to step II, either back to where it started or to Li-4. Only in the latter case, the Li hop contributes to Li current along the horizontal axis. Figure 2(d) shows the energy landscape in 16 NEB images along the diffusion path. We found that Li diffusion is a concerted motion with step I (and step III) spontaneously followed by step II (and step IV), where the group of Li atoms (Li-1 to Li-4) move simultaneously to bring the vacancy to its neighboring equivalent site (i.e., the site taken by Li-4 in Fig. 2(c)). The calculated E_A is 210 meV, which is 180 meV lower than the 390 meV for intercalated graphite (calculated at the same theoretical level). Other diffusion paths have higher barriers. For example, the hopping of Li-4 to the vacancy mediated by Li-5 (similar to the minimum-barrier path in Fig. 2(c)) has a barrier of 330 meV. Direct hopping of the vacancy to an equivalent neighboring site along *b* and *c* directions has a barrier of 510 and 480 meV, respectively. We found that the barrier height is correlated to the displacements of the Li atoms involved in the diffusion. In the minimum-barrier path, the displacement of Li atoms is from 2.57 to 2.85 Å, which are the smallest possible displacements. In other paths, the displacements are consistently longer. In particular, direct hopping involves the displacement of Li atoms of at least 4.58 Å, which explains the high diffusion barriers.

To understand the exceptionally low E_A, we recall how de-lithiation takes place in isolated molecule. When a Li is removed from either ends of the molecule (see Fig. 1(b) → Fig. 1(a)), an O dangling bond is created. The remaining Li ion is displaced noticeably towards the dangling bond until it is located at equal distance from either O. This bistability exists solely because of the resonant bonding of the COO ligand, as indicated in Fig. 1(a). When placed in a solid, despite the number of neighbors for the O ion is increased, a reminiscence of the resonant bonding may exist; namely, instead of being a saddle point at the transition state as one might expect, it becomes a local energy minimum that

effectively cut down the E_A. In the case of Li$_2$TPA, although we do not see a minimum, it is clear from Fig. 2(d) that an energy plateau exists along the diffusion path.

Motivated by the above analysis, we searched for other organic salt bulk materials that preserve the energy minimum at the transition state (and hence a lower E_A) and found that K$_2$TPA could be such a candidate. K$_2$TPA crystallizes in a different structure[23] from Li$_2$TPA (Fig. 3(a)) as a result of the large difference in ionic radii between K and Li. The structure for fully lithiated K$_2$TPA (or K$_2$TPA-Li$_2$) was obtained following the same method as that used for obtaining Li$_2$TPA-Li$_2$. Our searches based on both multiple starting configurations and simulated annealing lead to the same structure as shown in Fig. 3(b). Table I shows the optimized lattice parameters before and after lithiation. There is a difference in the structure changes between K$_2$TPA and Li$_2$TPA upon lithiation. While Li$_2$TPA shows volume decrease after lithiation, K$_2$TPA shows volume increase. The difference can be understood by comparing Figs. 2(b) and 3(b). In the case of Li$_2$TPA-Li$_2$, the added Li atoms form extra Li-O bonds, which result in shrinking of the lattice along **b** and **c** directions and decrease in volume. In the case of K$_2$TPA-Li$_2$, however, the Li atoms are inserted into the skeleton of the K-O bonds owing to the significant longer K-O bonds (2.81 Å on average) than the Li-O bonds (2.00 Å on average). The inserted Li atoms expand the lattice along **b** and **c** directions resulting in the volume increase. In view of the above mentioned structure difference, we re-examined the structure of Li$_2$TPA-Li$_2$ (Fig. 2(b)) by substituting all K atoms in K$_2$TPA-Li$_2$ (Fig. 3(b)) by Li atoms and then re-optimized the structure by variable-cell relaxation. The optimized structure, however, was found to be 0.58 eV/cell higher than the structure in Fig. 2(b). Further calculations using simulated annealing also confirmed the stability of the structure for Li$_2$TPA-Li$_2$ in Fig. 2(b).

TABLE I. Calculated lattice parameters of Li$_2$TPA and K$_2$TPA before and after lithiation, where a, b, and c are the lengths of the lattice vectors, β is the monoclinic angle, and Ω is the volume of the unit cell. Experimental values from Ref. 23 for Li$_2$TPA and K$_2$TPA before lithiation are also given.

	Li$_2$TPA		Li$_2$TPA-Li$_2$	K$_2$TPA		K$_2$TPA-Li$_2$
	This work	Experiment	This work	This work	Experiment	This work
a (Å)	8.49	8.36	8.86	10.54	10.56	9.73
b (Å)	5.14	5.13	4.73	4.09	3.94	4.34
c (Å)	8.89	8.49	8.70	11.72	11.54	12.32
β (°)	90.5	93.2	90.3	111.2	113.1	108.2
Ω (Å^3)	387.9	363.5	364.5	470.9	442.0	493.6

Li diffusion path in K$_2$TPA-Li$_2$ is also different from Li$_2$TPA-Li$_2$. In K$_2$TPA-Li$_2$, all Li sites (hence the vacancy sites) are equivalent. Due to the structural difference with Li$_2$TPA-Li$_2$, vacancy diffusion in K$_2$TPA-Li$_2$ involves only direct hopping of Li. Note that the energy profile here (see Fig. 3(d)) has a double hump with an energy minimum at nearly equal distance from the two O ions. This cuts down the E_A for K$_2$TPA-Li$_2$ to about 150 meV (240 meV lower than that in LiC$_6$) and confirms our resonant bond model for the low E_A. In contrast, E_A for K diffusion remains high. We have considered both K and Li vacancy diffusion mechanisms for K but found that E_A's $\geq$ 790 meV. This can be attributed to the larger ionic radius of K. Low K diffusion rate is beneficial, as it ensures the integrity and good cyclability of K$_2$TPA as an electrode material.

To assess the effects of vdW interaction, which strictly speaking cannot be accurately represented by PW91, we repeated the calculations with the DFT-D method. The DFT-D results are qualitatively the same as those from PW91; namely, much lower E_A for organic solids than that in Li-intercalated graphite. In particular, E_A in LiC$_6$ is 590 meV, while in Li$_2$TPA-Li$_2$ and K$_2$TPA-Li$_2$, it is 320 meV and 200 meV, respectively. This can be expected as resonant bonding is a property of the COO ligand and intrinsic to organic solids irrespective of the numerical details. In general, DFT-D gives better lattice parameters, as the method is optimized for them, while PW91 gives better anode voltage and E_A, as evidenced by the fact that E_A(PW91) of 390 meV in LiC$_6$ is in better agreement with measured Li diffusivity.[1]

We studied other properties of interest of the organic salts as anode materials, including the anode voltage, specific energy density, and volume change upon lithiation. We calculate the anode voltage for Li$_2$TPA by $V = [E(\text{Li}_2\text{TPA-Li}_2) - E(\text{Li}_2\text{TPA}) - 4 \times E(\text{bulk Li})]/4$,[27] where $E(\text{Li}_2\text{TPA-Li}_2)$ and $E(\text{Li}_2\text{TPA})$ are the total energy per unit cell after and before the lithiation, and $E(\text{bulk Li})$ is the total energy per Li in the bulk *bcc* phase. A factor 4 enters because each Li$_2$TPA primitive cell can accommodate four inserted Li atoms. Because the contribution from entropy and volume changes are negligible,[27,28] here we used the total energy instead of the Gibbs free energy. The calculated anode voltage is 0.73 V under full lithiation, which is reasonably close to the experimental value of 0.8 V.[9] The calculated anode voltage for K$_2$TPA is 0.62 V, lower than that of Li$_2$TPA. Despite that this voltage is still higher than that of graphite, it is among the lowest in anode materials currently under study, such as

FIG. 3. (Color online) Crystal structure of K$_2$TPA before (a) and after (b) lithiation. Atom coloring scheme is the same as that in Fig. 2 except that K atoms are denoted by purple (large gray in black-and-white print version) balls. (c) Diffusion path of Li vacancy in K$_2$TPA-Li$_2$. Open circle represents the initial Li vacancy. Dashed line encloses one K$_2$TPA-Li$_2$ unit with a Li vacancy. (d) Potential energy curve along the diffusion path.

$Li_4Ti_5O_{12}$.[29] The specific energy density of K_2TPA (209 mA·h/g) is lower than that of Li_2TPA (279 mA·h/g) because of the higher atomic weight of K. We note that the bottleneck on the specific energy density in LIBs is usually the cathode material as they often involve heavier transition elements. For example, the most commonly used cathode materials $LiCoO_2$ and $LiFePO_4$ have a specific energy density of 140 and 170 mA·h/g, respectively.[29] It is important to note that due to the weak vdW binding between TPAs, organic salts have plenty room to accommodate Li insertion without significant volume change, which is highly desirable for electrode materials. In particular, we found an overall volume change of only -6.0% and $+4.8\%$, respectively, after full lithiation of Li_2TPA and K_2TPA. The details of the structure changes are summarized in Table I.

In summary, using first-principles calculations, we studied organic salts Li_2TPA and K_2TPA as potential LIB electrode materials. These materials are found to have intrinsically high Li diffusion rates. In particular, E_A in K_2TPA is only 150 meV, which is 240 meV lower than that in state-of-the-art Li-intercalated graphite and corresponds to four orders of magnitude higher Li diffusion rate at room temperature. Resonant bonding in organic salts, which results in an intrinsic Li bistability upon de-lithiation, is identified as the mechanism for the remarkably low E_A's. Our findings call for further investigation of organic salts, both TPA-based and beyond, for power-intensive battery applications not only as anode but also as cathode materials.

[1] K. Persson, V. A. Sethuraman, L. J. Hardwick, Y. Hinuma, Y. S. Meng, A. van der Ven, V. Srinivasan, R. Kostecki, and G. Ceder, J. Phys. Chem. Lett. **1**, 1176 (2010).
[2] K. Toyoura, Y. Koyama, A. Kuwabara, and I. Tanaka, J. Phys. Chem. C **114**, 2375 (2010).
[3] M. Okubo, Y. Tanaka, H. Zhou, T. Kudo, and I. Honma, J. Phys. Chem. B **113**, 2840 (2009).
[4] P. L. Taberna, S. Mitra, P. Poizot, P. Simon, and J. M. Tarascon, Nature Mater. **5**, 567 (2006).
[5] M. Okubo, E. Hosono, J. Kim, M. Enomoto, N. Kojima, T. Kudo, H. Zhou, and I. Honma, J. Am. Chem. Soc. **129**, 7444 (2007).
[6] Y. Li, B. Tan, and Y. Wu, Nano Lett. **8**, 265 (2008).
[7] C. K. Chan, H. Peng, G. Liu, K. McIlwrath, X. F. Zhang, R. A. Huggins, and Y. Cui, Nat. Nanotechnol. **3**, 31 (2008).
[8] K. Kang, Y. S. Meng, J. Breger, C. P. Grey, and G. Ceder, Science **311**, 977 (2006).
[9] M. Armand, S. Grugeon, H. Vezin, S. Laruelle, P. Ribiere, P. Poizot, and J. M. Tarascon, Nature Mater. **8**, 120 (2009).
[10] G. Kresse and J. Hafner, Phys. Rev. B **47**, 558 (1993).
[11] G. Kresse and J. Furthmüller, Comput. Mater. Sci. **6**, 15 (1996).
[12] G. Kresse and D. Joubert, Phys. Rev. B **59**, 1758 (1999).
[13] J. P. Perdew, J. A. Chevary, S. H. Vosko, K. A. Jackson, M. R. Pederson, D. J. Singh, and C. Fiolhais, Phys. Rev. B **46**, 6671 (1992).
[14] J. R. Dahn, Phys. Rev. B **44**, 9170 (1991).
[15] K. Persson, Y. Hinuma, Y. S. Meng, A. Van der Ven, and G. Ceder, Phys. Rev. B **82**, 125416 (2010).
[16] K. R. Kganyago and P. E. Ngoepe, Phys. Rev. B **68**, 205111 (2003).
[17] Y. Zhang, W. Pan, and W. Yang, J. Chem. Phys. **107**, 7921 (1997).
[18] S. Grimme, J. Comput. Chem. **27**, 1787 (2006).
[19] P. E. Blöchl, Phys. Rev. B **50**, 17953 (1994).
[20] M. Methfessel and A. T. Paxton, Phys. Rev. B **40**, 3616 (1989).
[21] O. H. Nielsen and R. M. Martin, Phys. Rev. B **32**, 3780 (1985).
[22] M. C. Payne, M. P. Teter, D. C. Allan, T. A. Arias, and J. D. Joannopoulos, Rev. Mod. Phys. **64**, 1045 (1992).
[23] J. A. Kaduk, Acta Crystallogr. B **56**, 474 (2000).
[24] G. Henkelman, B. P. Uberuaga, and H. Jónsson, J. Chem. Phys. **113**, 9901 (2000).
[25] G. Henkelman and H. Jónsson, J. Chem. Phys. **113**, 9978 (2000).
[26] Y. S. Meng and M. E. A. de Dompablo, Energy Environ. Sci. **2**, 589 (2009).
[27] G. Ceder, M. K. Aydinol, and A. F. Kohan, Comput. Mater. Sci. **8**, 161 (1997).
[28] J. N. Reimers and J. R. Dahn, Phys. Rev. B **47**, 2995 (1993).
[29] B. Scrosati and J. Garche, J. Power Sources **195**, 2419 (2010).